Hindawi
Geofluids
Volume 2024, Article ID 2387180, 18 pages
https://doi.org/10.1155/2024/2387180

Research Article

Genesis of the Early Indosinian Darongshan Granitoid in South China: Response to the Subduction of the Eastern Paleo-Tethys Ocean

Meng-Yu Tian,[1] Yong-Jun Di,[2] Chun-Yu Zhang,[2] and Shu-Guang Deng[3]

[1]*School of Resources and Environmental Engineering, Hefei University of Technology, Hefei, China*
[2]*School of Earth Science and Mineral Resources, China University of Geosciences (Beijing), Beijing, China*
[3]*School of Geography and Planning, Nanning Normal University, Nanning, China*

Correspondence should be addressed to Yong-Jun Di; diyongjun@cugb.edu.cn

Received 22 September 2023; Revised 22 December 2023; Accepted 6 January 2024; Published 25 January 2024

Academic Editor: Farhad Ehya

The Bangxi–Chenxing suture zone is an essential area from which information about the closure history of the eastern Paleo-Tethys Ocean can be obtained. The Darongshan granitoid, which is adjacent to this suture, lies among the widely distributed granitic rocks and few basic rocks in the southern Guangxi Province. Herein, we report the petrogeochemistry, zircon U–Pb ages, and zircon Hf isotopic data of the Darongshan pluton in this region. The LA-ICP-MS U–Pb zircon analysis indicates that the Darongshan pluton had formed at 249.9 ± 2.6 Ma. The Darongshan granites are silica-rich (SiO_2 = 65.68 – 72.91 wt%, mean = 69.89 wt%) with high Na_2O contents (Na_2O = 0.46 – 6.58 wt%, mean = 3.49), relatively high Mg ($Mg^{\#}$ = 35.12 – 73.31, mean = 57.73), and an average $Fe_2O_3{}^{T}$+TiO_2+MnO+MgO of 4.96. These features are similar to those of the Mg-andesitic/dioritic rock- (MA-) like tonalite–trondhjemite–granodiorites (TTGs). Chemical analyses show that all rocks are enriched in large-ion lithophile elements (Rb, Th, and U) and light rare earth elements, with weak negative Eu anomalies (Eu/Eu^{*} = 0.27 – 0.67), and Ta, Nb, and Ti depletion, with typical arc-like affinity. The zircon Hf isotopic results show zircon $\varepsilon_{Hf}(t)$ values ranging from -18.2 to -7.4 and the T_{DM2} model ages 1.74–2.41 Ga. The petrogeochemistry and zircon Hf isotopic signatures indicate the magma generation of the Darongshan granitoid with fluid/melt released from the subducted slab and the fluid/melt assimilated and mixed with the mantle peridotite during ascent. Combining previous extant information on Permo–Triassic subduction/collision-related magmatism in the Bangxi–Chenxing with that of the Jinshajiang–Ailaoshan–Song Ma suture zones, the Darongshan granitoid is interpreted as a magmatic formation that was generated in an active continental margin arc environment during the subduction of the Early Indosinian eastern Paleo-Tethys Ocean and the South China Block, further supporting the idea that closure occurred during the Middle–Late Triassic.

1. Introduction

The Paleo-Tethys Ocean is the major ocean that formed between the continental fragments of Southeast Asia and the Eastern Cimmerian supercontinent, extending from the European Alps to the Southwest China and Southeast Asia [1–3]. In Southeast Asia, the ocean is referred to as the East Paleo-Tethys Ocean. The remnant oceanic and subduction-related fragments, tectonically named the East Paleotethyan belt, extends from Nepal, India, and southwest Yunnan to the Malay Peninsula [4–6], with the Jinshajiang–Ailaoshan–Song Ma suture zone in Southeast Asia, an important crustal boundary between the Indochina and South China blocks that represents the closure of one branch of the Paleo-Tethys Ocean (Figure 1; [7–9]). Recent research has indicated that the Bangxi–Chenxing ophiolite is an eastern extension of the Song Chay suture in Northeast Vietnam [10–12] and the easternmost segment of the Paleo-Tethys Ocean may have been an extension of the Song Ma suture zone, which extends through the Qiongzhou Strait to central Hainan Island [13–16]. However, the current understanding of the subduction and collisional processes differs, and it

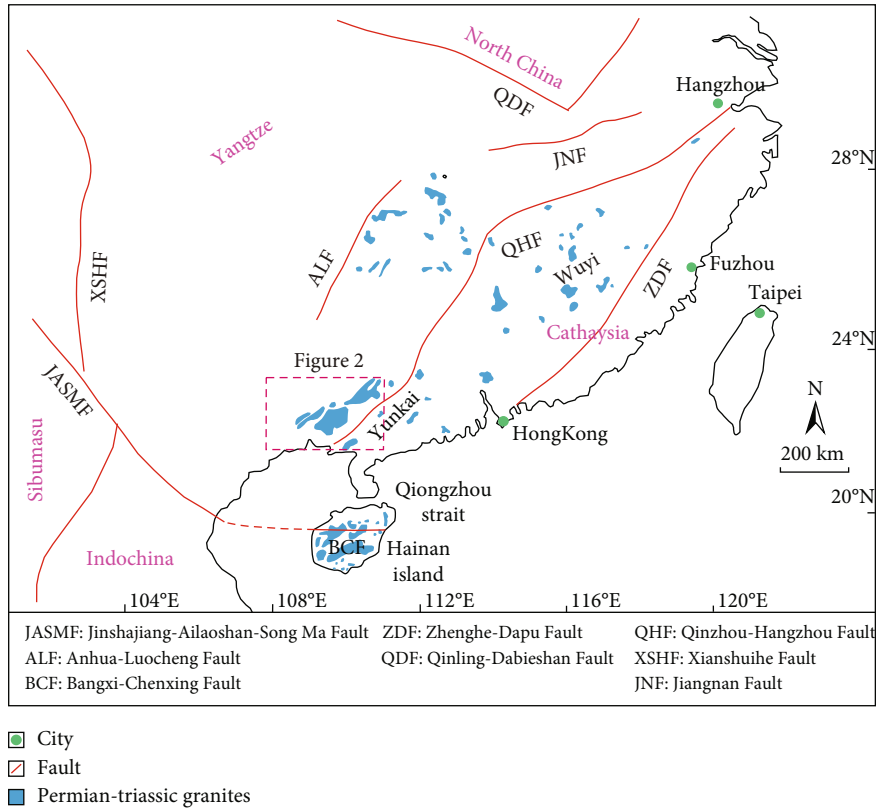

Figure 1: Distribution map of Permian–Triassic magmatic rocks in South China (modified after [36, 46]).

remains unknown whether (1) the closure of the eastern Paleo-Tethys Ocean occurred in the Middle Permian (269–263 Ma; [17]), Late Permian–Earliest/Middle Triassic [15, 18, 19], or Middle Triassic [8, 20, 21] or (2) whether the plate subduction during the closure of the eastern Paleo-Tethys Ocean was double-sided [17] or occurred in a northward [19, 21, 22] or southward [18, 23] direction. One major factor influencing these debates is the lack of information concerning the arc magmatism in association with subduction in the northern part of the Bangxi–Chenxing ophiolite.

The Bangxi–Chenxing suture zone is located in the southwestern part of the South China Block (SCB) (Figure 1), which is a part of the eastern section of the Paleo-Tethys tectonic domain and is connected to the Paleo-Pacific tectonic domain [24]. Although the Bangxi–Chenxing suture zone has undergone multiple phases of magmatism, with multiple tectonic-magmatic phases, scant evidence of magmatism in association with the closing of the eastern Paleo-Tethys Ocean is available. Therefore, the understanding of the tectono-magmatic evolution that is associated with this process remains poor.

Magmatic suites with rock assemblages provide significant constraints on both geodynamic processes and tectonic settings. For example, tonalite–trondhjemite–granodiorites (TTGs), Mg/high-Mg andesites/diorites, and adakitic rocks are usually associated with subduction-related environments (e.g., [25–27]). TTGs are silica-rich ($SiO_2 > 64$ wt%, commonly ~70 wt% or greater) with high Na_2O contents (3.0–7.0 wt%) and are poor in ferromagnesian elements ($Fe_2O_3{}^T + TiO_2 + MnO + MgO \leq 5$ wt%), with average Cr and Ni contents of 40 and 18 ppm, respectively (e.g., [28, 29]). In particular, Mg-andesitic/dioritic rock (MA)-like TTGs usually develop in subducted oceanic crust along convergent plate margins. Therefore, studying the assemblages is essential for rebuilding oceanic plate subduction, crust–mantle interaction, and continental crust evolution.

This study is focused upon the Darongshan pluton complex in the northern part of the Bangxi–Chenxing ophiolite. The results of the newly obtained petrological, whole-rock geochemical, zircon chronology, and Hf isotope data allow to constrain the petrogenetic and tectonic settings of the MA-like TTGs in the Darongshan pluton and provide important petrological evidence of the closure of the eastern Paleo-Tethys Ocean.

2. Geological Setting and Pluton Features

The SCB consists of the Cathaysia Block in the southeast and Yangtze Block in the northwest, which are assumed to have amalgamated during the Neoproterozoic (Figure 1; [16, 24] and references therein). The Cathaysia Block is characterized by the extensive generation of magmatic rocks (e.g., [9, 18, 30]), with the ages at which the granitic rocks intruded roughly divided into the Early Paleozoic (ca. 460–400 Ma), Permian–Triassic (ca. 270–230 Ma), and Jurassic–Cretaceous (ca. 180–80 Ma) [31–33]. South China collided with Indochina to the south and North China to the north during the Triassic [34], resulting in unconformities, deformation,

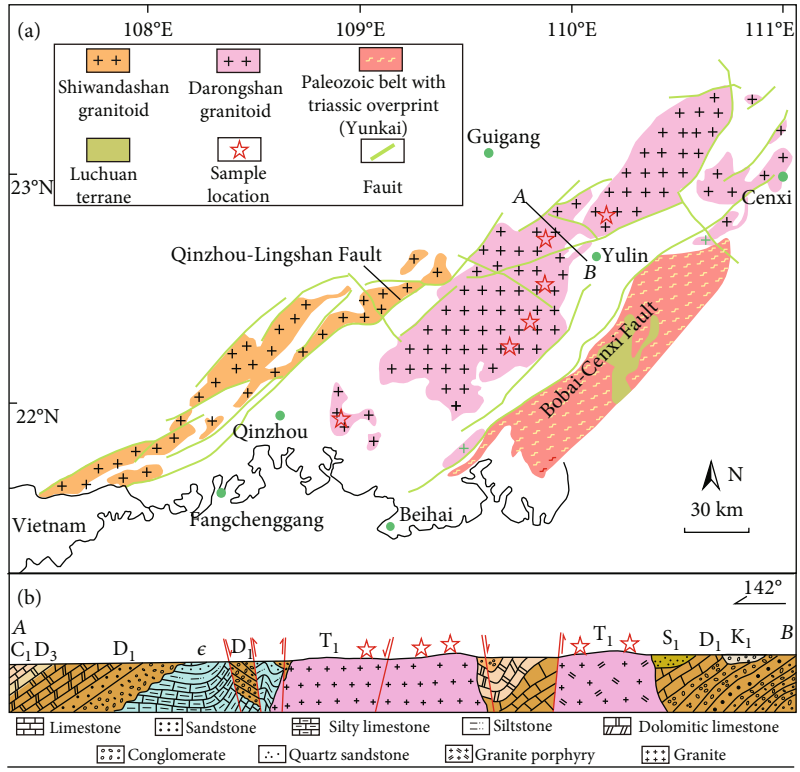

FIGURE 2: (a) Geological map of southeastern Guangxi (modified after [38]). (b) Schematic cross section (location shown in (a)) of the Darongshan pluton showing the structural relationships among the different lithological units.

and orogenic magmatism, indicating strong tectonic processes [35–37]. The Triassic granitic rocks of South China are mainly high-K calc-alkaline, weakly peraluminous, and predominantly I- and S-type granites, with a few A-type granites [38].

The Darongshan pluton includes several Early Triassic granite batholiths, such as Darongshan, Pubei, and Nali. These batholiths are distributed over an area of >7000 km^2 within Guangxi Province and are elongated in a NE–SW (ca. 350 km) with variable width (25–70 km) (Figure 2(a); [39, 40]). The Darongshan pluton is mainly composed of biotite monzogranite, granite–porphyry, and a small amount of migmatitic granite (e.g., [17, 41]). The ages of these granites vary greatly, ranging 260–230 Ma, as determined by SHRIMP and LA-ICP-MS U–Pb zircon dating and EMP U–Th–Pb monazite dating [42–44]). Jiao et al. [38] obtained a uniform emplacement age of ca. 250 Ma for each suite in the Darongshan granitoid using SIMS U–Pb zircon dating.

The Darongshan pluton has intruded into the Cambrian, Silurian, Devonian, and Lower–Middle Carboniferous strata with irregular contact relationships and is overlain by Late Triassic and Jurassic sediments (Figure 2(b); Figures 3(a)–3(e); [36, 45]). Hornfels have developed locally at the contact area between the granite–porphyry and strata from the Silurian Liantan Formation (S_1l), which is composed of quartz sandstones and siltstone/slates with minor sandstone interlayers (Figure 3(a); [24, 45]). Partial thermal metamorphism can be seen in the contact zone between the granite and Devonian Lianhuashan Formation strata (D_1l), which is composed of conglomerates, reddish purple quartz sandstones, and shales (Figure 3(d); [46]). In addition to the intrusion, fault contact is observed where the granite contacts Carboniferous strata. Normal faults have developed with a strike of approximately 50–65° and a dip angle of approximately 80° (Figure 3(e)). Moreover, the granites contain numerous, irregularly arranged mafic microgranular enclaves (Figure 3(f)).

3. Petrography

Two groups of granitoid samples were collected from the Darongshan pluton according to the different types of granite units and contact relationships, ensuring that the main characteristics of the pluton are represented.

The samples from the first group are characterized by medium-grained hypersthene granite–porphyry and consist of quartz (20–25%), K-feldspar (10–15%), and plagioclase (15–20%), with small amounts of biotite (5–10%) and hypersthene (5–8%) (Figure 4). The matrix is cryptocrystalline (15–20%). The biotite and feldspar are subhedral, and the quartz is anhedral (Figure 4). The K-feldspar phenocrysts range 0.5–1.5 mm with no twinning (Figures 4(a)–4(d)), while plagioclase phenocrysts show polysynthetic twinning and oscillatory zoning, with K-feldspar and quartz inclusions (Figures 4(c) and 4(d)). Hypersthene ranges 0.5–1.5 mm and is often observed alongside the plagioclase

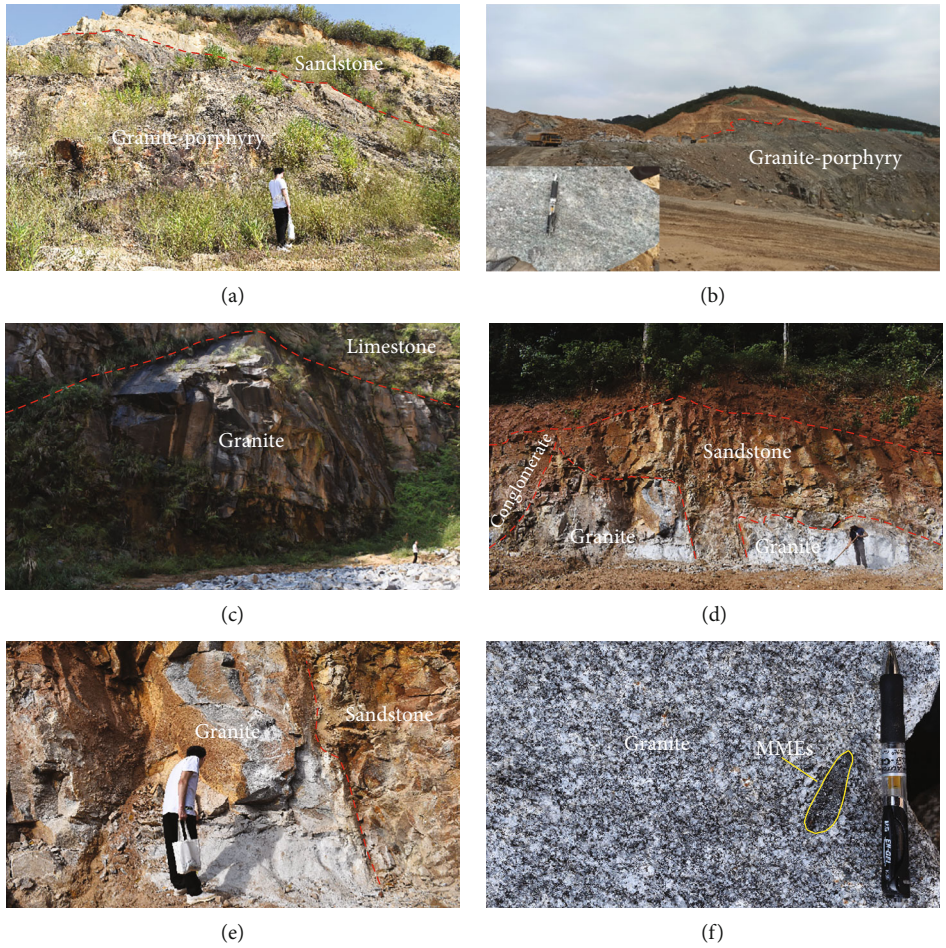

Figure 3: Field photographs: (a) Granite–porphyry intruded into sandstone formations; (b) granite–porphyry overlain by Late Mesozoic strata; (c) granite intruded into limestone formations; (d) granite intruded into Devonian Lianhuashan Formation strata (D_1l); (e) fault contact; (f) potassic granite with mafic microgranular enclaves (MMEs).

phenocrysts (Figures 4(e)–4(h)). The accessory minerals are garnet (Figures 4(a) and 4(b)), zircon, and monazite.

Samples from the second group are characterized as medium- to coarse-grained granite and consist of quartz (20–25%), K-feldspar (15–20%), plagioclase (20–25%), and biotite (8–10%), with minor amounts of cordierite (3–5%) (Figure 5). Anhedral quartz ranges 0.5–3.5 mm, and quartz includes feldspar grains (Figures 5(a)–5(d)). Subhedral K-feldspar and plagioclase range 0.5–2.5 mm (Figures 5(c) and 5(d)), and the plagioclase shows oscillatory zoning with a few weak secondary changes (Figures 5(c)–5(f)). The biotite is dark brown with a flakey structure, and the secondary alteration is mainly weak sericitization (Figures 5(a)–5(f)). The accessory minerals included zircon, garnet, and titanite (Figures 5(e)–5(h)).

4. Analytical Methods

Analysis of the major, trace, and rare earth elements within the Darongshan granitoids was completed at the Key Laboratory of Orogenic Belts and Crustal Evolution, Peking University, China. The major elements were measured by the flax method and analyzed using a scanning wavelength-dispersive X-ray fluorescence spectrometer (AR-LAD-VANTXP+) with an error of less than 5%. Trace and rare earth elements were analyzed using an Agilent 7500ce inductively coupled plasma mass spectrometer (ICP-MS) for which 25 mg powder samples were placed in a Teflon beaker with 2 mL Hf (40%), 0.6 mL HNO_3 (68%), and 0.5 mL $HClO_4$ (72%), which was then sealed, heated in an electric oven at 185°C for 72 h, and left for evaporation. Another 1–2 mL of HNO_3 (68%) was then added, and the solution evaporated until dry. This step was then repeated, and the obtained residue was redissolved in 10 mL HNO_3 (2%) before sealing and heating in an electric oven at 105°C for 12 h. The obtained solution was then diluted to 25 mL using HNO_3 (2%) solution for ICP-MS measurements. The measurement precision was greater than 5%, and the analytical values for all elements showed <10% error as compared to the standard values.

A fresh Darongshan granitoid sample (YK021-1) was selected for zircon dating. Zircon sorting was performed by the Langfang Geoscience Exploration Technology Service Co., Ltd., and zircon target preparation, cathodoluminescence

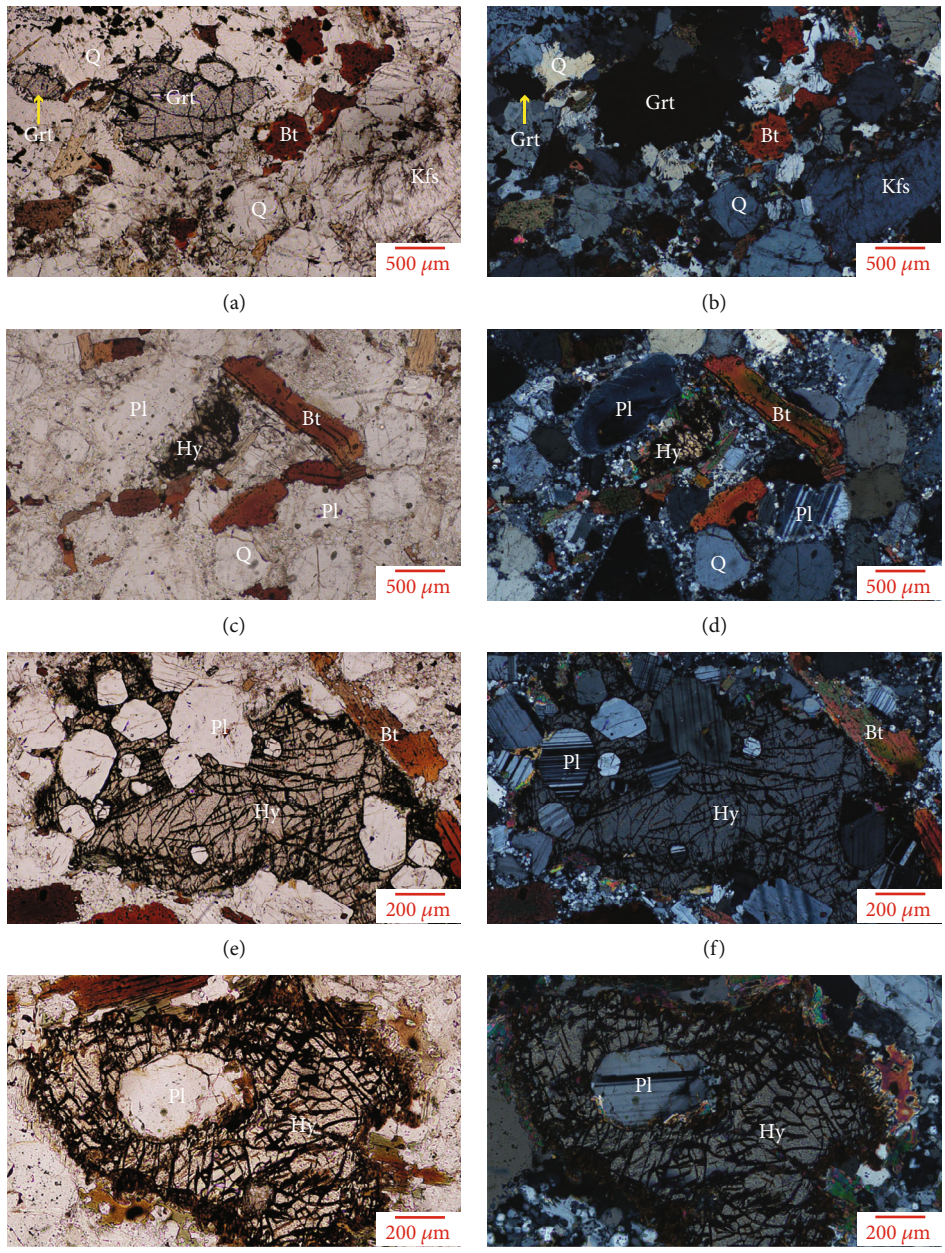

Figure 4: Petrographic characteristics of hypersthene granite–porphyry samples from the Darongshan pluton: (a, b) photographs of quartz, K-feldspar, plagioclase, biotite, and garnet; (c, d) plagioclase develops polysynthetic twinning and a few weaker secondary changes; (e–h) plagioclase are encased in hypersthene. Mineral abbreviations: Q = quartz; Kfs = K-feldspar; Pl = plagioclase; Bt = biotite; Hy = hypersthene; Grt = garnet.

micrography (CL), and LA-ICP-MS zircon U–Pb dating were performed by Beijing GeoAnalysis Co., Ltd. Zircons were photographed using a JSM6510 scanning electron microscope (JEOL Corporation, Japan). An NWR193UC model laser ablation system (Elemental Scientific Lasers LLC, USA) was coupled with an Agilent 7900 ICP-MS instrument (Agilent, USA) at 6 Hz and a fluence of 5 J/cm^2 for the analysis of 30 μm spots. Iolite software was used for data reduction [36]. Zircons GJ-1 and 91500 were used as primary and secondary reference materials, respectively, and GJ-1, 91500, and Plešovice were analyzed twice, once every 10 sample analyses. Typically, 45 s sample signals were acquired after 25 s gas background measurements, with exponential functions used to calibrate the downhole fractionation. Further details of the process used can be found in literature [47–49].

Zircon Lu–Hf isotopic composition analyses were conducted at Beijing GeoAnalysis Co., Ltd. (Beijing, China), using a RESO 193 nm laser ablation system (Australian Scientific Instruments, Canberra, Australia) and a Neptune

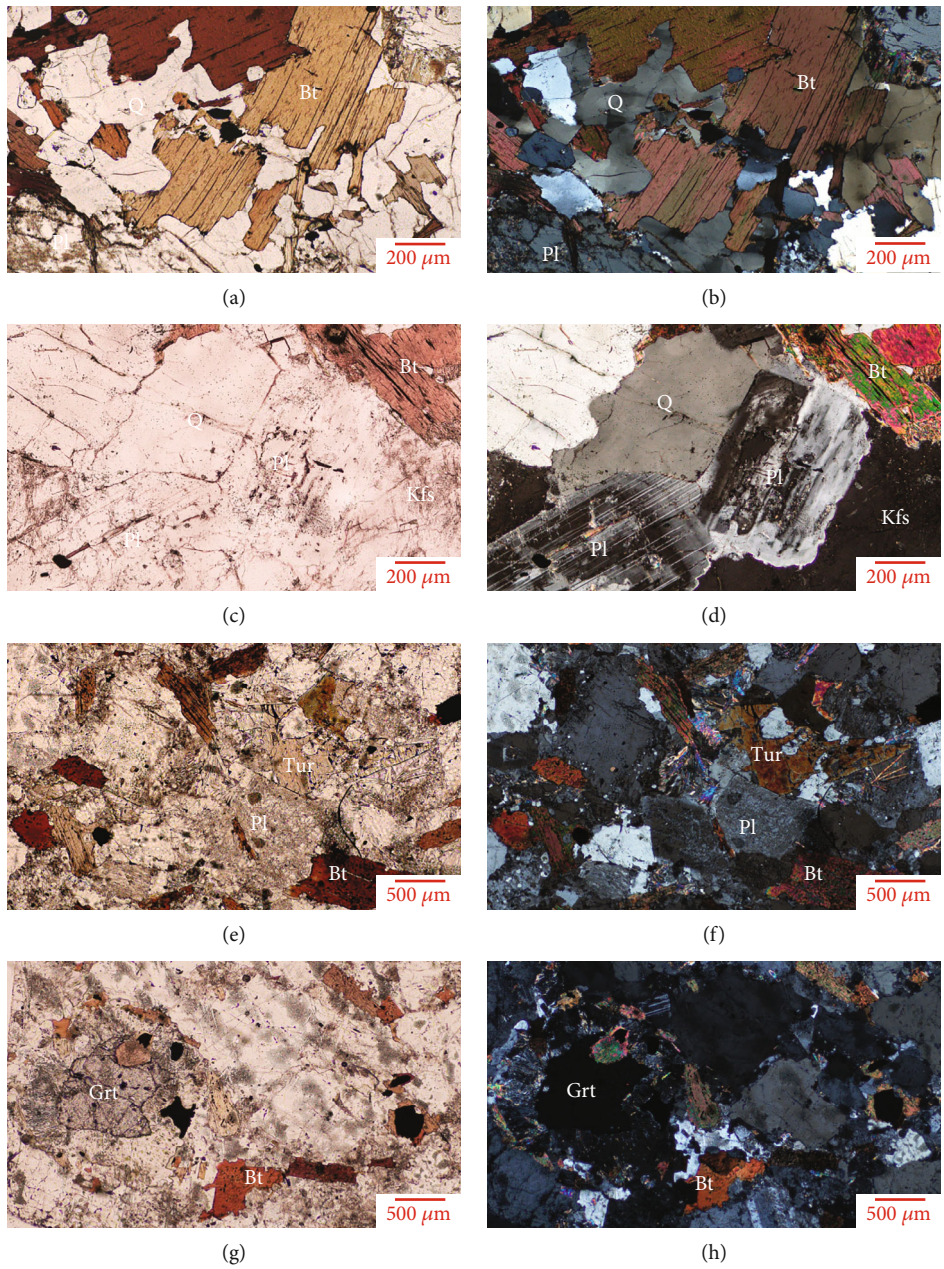

FIGURE 5: Petrographic characteristics of granite samples from the Darongshan pluton: (a–d) photographs of quartz, K-feldspar, plagioclase, and biotite; (e–h) Photographs of tourmaline and garnet. Mineral abbreviations: Q = quartz; Kfs = K-feldspar; Pl = plagioclase; Bt = biotite; Tur = tourmaline; Grt = garnet.

Plus MC-ICP-MS (Thermo Fisher Instruments, USA). Ablation was conducted using helium as the carrier gas and a laser beam spot with a diameter of 40 μm. The internationally accepted standard zircon Plešovice was used as reference material [49]. Further details of the analytical procedures used are described in Wu et al. [50]. The $^{176}Hf/^{177}Hf$ of 0.282480 ± 0.000016 (2σ) that was obtained for the standard zircon Plešovice is consistent with the value obtained previously and was within an acceptable error range [51]. The $^{176}Hf/^{177}Hf$ and $^{176}Lu/^{177}Hf$ ratios of 0.0332, 0.282772 and 0.0384, 0.28325 that were obtained for present-day chondrite and depleted mantle, respectively [52], were used to calculate the $\varepsilon_{Hf}(t)$ values. The two-stage Hf model ages (T_{DM2}) were calculated using $^{176}Lu/^{177}Hf = 0.015$ for average continental crust [51].

5. Results

5.1. Major and Trace Element Geochemistry. The abundances of major and trace elements in the Darongshan granitoids are shown in Table S1. The Darongshan granitoids show medium–high SiO_2 (65.68–73.33 wt%), high concentrations of Al_2O_3 (12.54–17.62 wt%), and low TiO_2 (0.07–0.87 wt%) and are alkaline-rich (with $K_2O + Na_2O =$

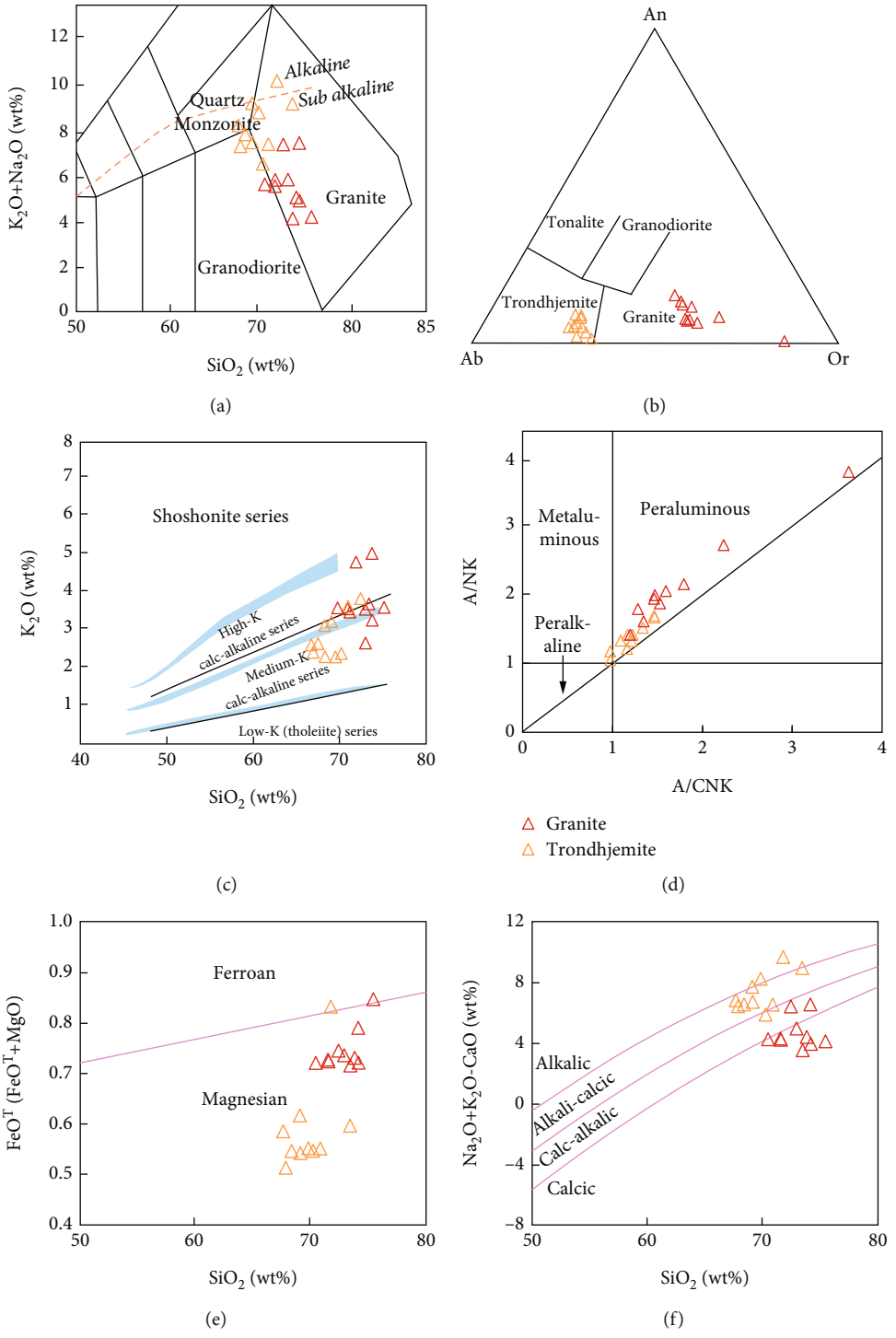

Figure 6: Geochemical classification diagrams of granitoid samples from the Darongshan pluton: (a) total alkalis versus silica diagram (after [114]); (b)An–Ab–Or diagram (after [115]); (c) K_2O vs. SiO_2 diagram (after [116]); (d) A/NK vs. A/CNK diagram (after [117]). A/CNK–molar (Al_2O_3/(CaO+Na_2O+K_2O)); A/NK-molar (Al_2O_3/(Na_2O+K_2O)); (e) SiO_2 vs. FeO^T/(FeO^T+MgO) diagram; (f) SiO_2 vs. Na_2O+K_2O–CaO (MALI) diagram. Boundaries between magnesian and ferroan and alkali, alkali-calcic, calc-alkalic, and calcic are from Frost et al. [118]. Data sources are referenced in Table S1 of the Supplementary Materials.

4.08 – 10.16 wt%), with Na_2O/K_2O ratios of 0.13–2.15. The samples in the total alkali-silica (TAS) diagram plot lie mainly in the granite field (Figure 6(a)). Based on normative mineral classification, all samples clearly are plotted on the trondhjemite and granite fields in the An–Ab–Or diagram (Figure 6(b)), and most samples are high-K and medium-K calc-alkaline in the SiO_2 vs. K_2O diagram (Figure 6(c)). Most samples are located in the

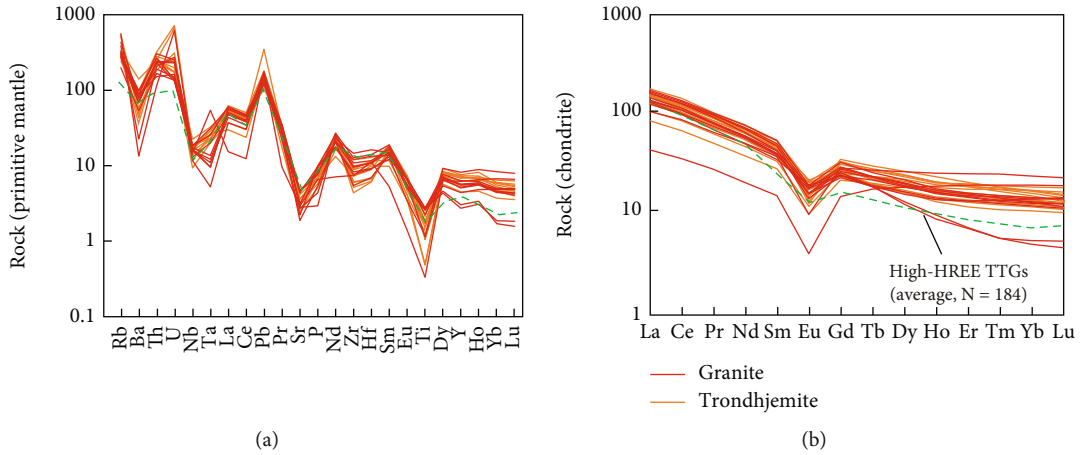

FIGURE 7: Chondrite-normalized REE patterns (a) and primitive mantle-normalized trace element patterns (b) of granitoid samples from the Darongshan pluton. Normalizing data are from Sun and McDonough [119]. High-HREE TTGs (average, $N = 184$) data are from Martin and Moyen [120] and Moyen [61].

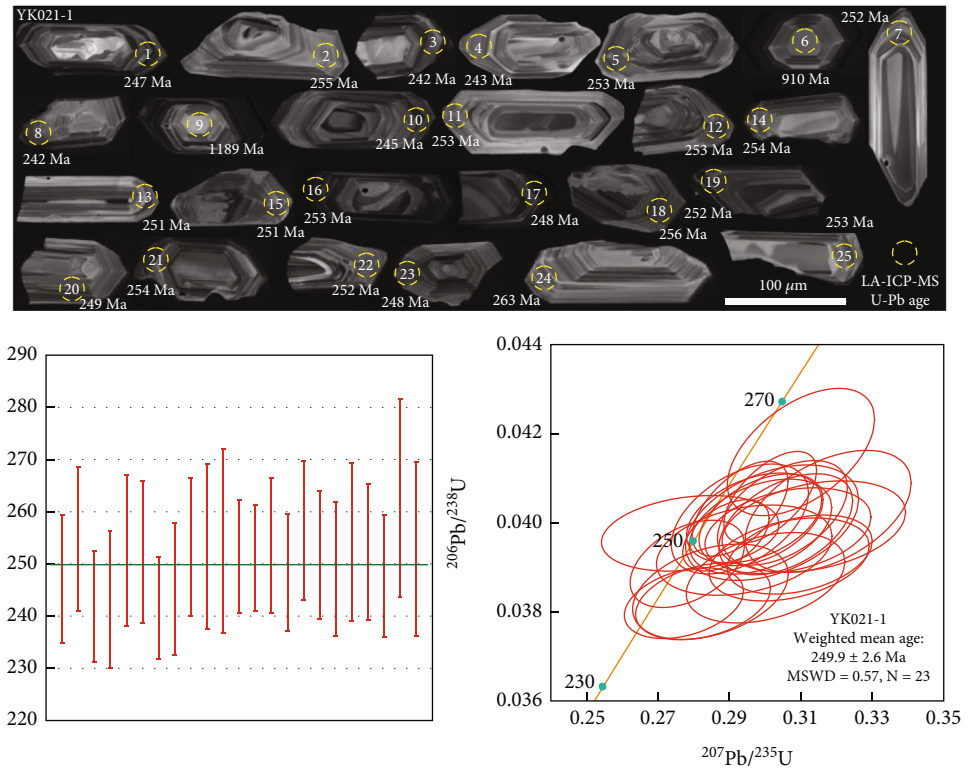

FIGURE 8: Zircon cathodoluminescence images and concordia diagram of samples (YK021-1) from the Darongshan pluton. Data sources are referenced in Table S2 of the Supplementary Materials.

peraluminous field, with a few in the metaluminous field (A/CNK = 0.96 – 3.61, A/NK = 1.04 – 3.77, Figure 6(d)). The SiO_2 vs. $FeO^T/(FeO^T+MgO)$ and Na_2O+K_2O–CaO diagrams (Figures 6(e) and 6(f)) indicate that the Darongshan granitoids are magnesian granites with characteristics ranging from calcic to alkali-calcic.

The trace and rare earth element characteristics of the Darongshan granitoids are remarkably similar. The total rare earth elements (REE) are in the range 65.92–213.88 ppm (with a mean value of 168.29 ppm, Table S1) for all samples, with LREE/HREE (LREE: light rare earth elements; HREE: heavy rare earth elements) ratios of 2.76–13.77 (mean value of 8.11). The $(La/Yb)_N$ values range 2.26–32.53, with an average value of 11.52, indicating fractionation of the LREE and HREE. All samples are LREE-enriched, with moderately negative Eu anomalies

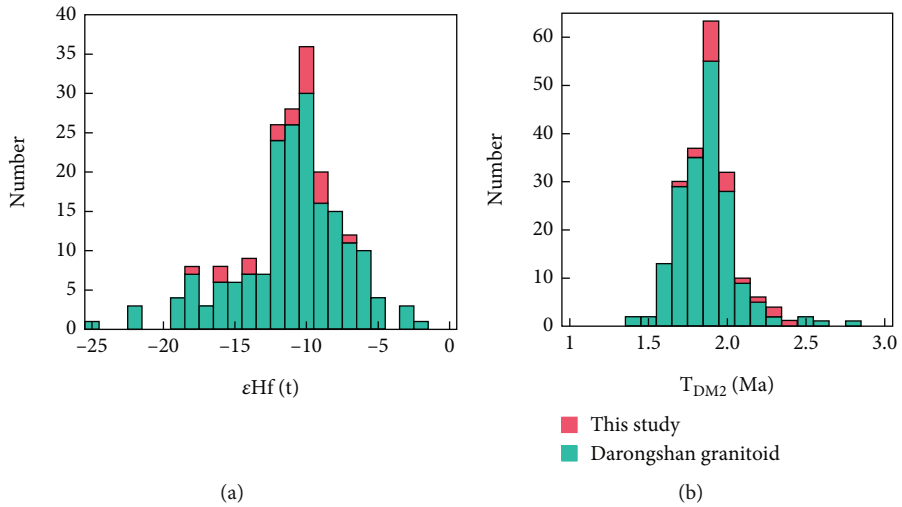

FIGURE 9: (a) Histogram of zircon $\varepsilon_{Hf}(t)$ and (b) $T_{DM2}(Hf)$ values for the granitoid samples from the Darongshan pluton. Data sources are referenced in Table S3 and Table S6 of the Supplementary Materials.

(Eu/Eu* = 0.27 – 0.67, Figure 7(a)). The primitive mantle-normalized trace element diagrams (Figure 7(b)) indicate that all rock samples are enriched in the large-ion lithophile elements (LILE; e.g., Rb, Th, and U) and depleted in the high-field-strength elements (HFSE; e.g., Ta, Nb, and Ti), indicating typical arc-like characteristics for the granitoid.

5.2. Zircon U–Pb Ages. The geochronological data presented in Table S2 was obtained from 25 analytical procedures that were performed on sample YK021-1 from the Darongshan granitoid. The zircons in the sample are euhedral to subhedral, long, prismatic, colorless, and transparent, with lengths ranging 30–150 μm and aspect ratios of 1 : 1–4 : 1. CL imaging revealed clear oscillatory zoning in all grains, with typical magmatic characteristics (Figure 8). The Th content ranged 72–687 ppm and the U content 222–1752 ppm, with the Th/U ratio varying 0.11–0.64 with an average of 0.34. The $^{206}Pb/^{238}U$ age obtained from spot analysis ranged 1189 ± 12–242 ± 2 Ma (Table S2), with 23 of the results yielding a $^{206}Pb/^{238}U$ age of 249.9 ± 2.6 Ma (MSWD = 0.57) (excluding results YK021-1-06 and YK021-1-09; see Figure 8). It should be noted that sample YK037 also showed a zircon U–Pb age of 250.1 ± 2.6 Ma (our published data, [53]).

5.3. Zircon Hf Isotopic Composition. The zircon Hf isotopic compositions of YK021-1 and YK037 were then analyzed and the results given in Table S3. The results show an $\varepsilon_{Hf}(t)$ that is between -18.2 and -7.4, with an average of -11.38; a T_{DM} that varies between 1.21 and 1.62 Ga, with an average of 1.36 Ga; and a T_{DM2} that ranges from 1.74 to 2.41 Ga, with an average of 1.99 Ga (Table S3). The Darongshan granitoid exhibits $\varepsilon_{Hf}(t)$ values ranging from -24.9 to -1.8, with a peak at -10.0 (Figure 9(a)), and the corresponding Hf isotopic model ages ($T_{DM2}(Hf)$) range from 1.4 to 2.8 Ga, with a peak at 1.9Ga (Figure 9(b)).

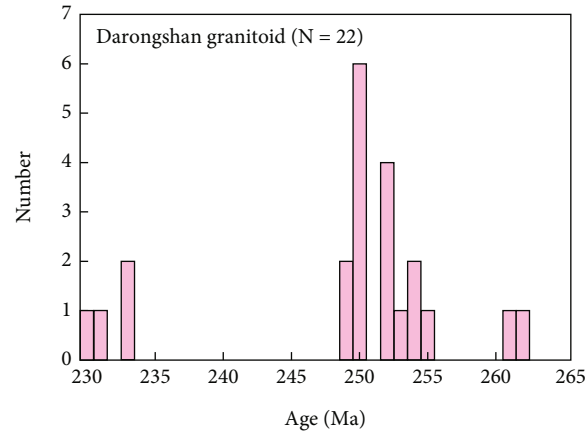

FIGURE 10: Histogram of age values for the granitoid samples from the Darongshan pluton. Data sources are referenced in Table S4 of the Supplementary Materials.

6. Discussion

6.1. Age of the Darongshan Granitoid. Magma crystallization ages of 249.9 ± 2.6 Ma and 250.1 ± 2.6 Ma were obtained for samples YK021-1 and YK037 from the Darongshan granitoid (our published data, [53]), respectively. Age data for the Darongshan pluton have been obtained using different zircon U–Pb dating methods (Table S4), with zircon U–Pb ages for the Darongshan pluton ranging from 262 to 230 Ma, with a peak age of ca. 252 Ma (Figure 10). This peak age is similar to that of the Darongshan granitoids in this study. Combining these geochronological data, we suggest that the Darongshan pluton may have formed at approximately 255–250 Ma.

6.2. Petrogenesis of the Darongshan Granitoids. The Darongshan granitoids are silica-rich (SiO_2 = 65.68 – 72.91 wt%, mean = 69.89 wt%) with high Na_2O content (Na_2O = 0.46 –

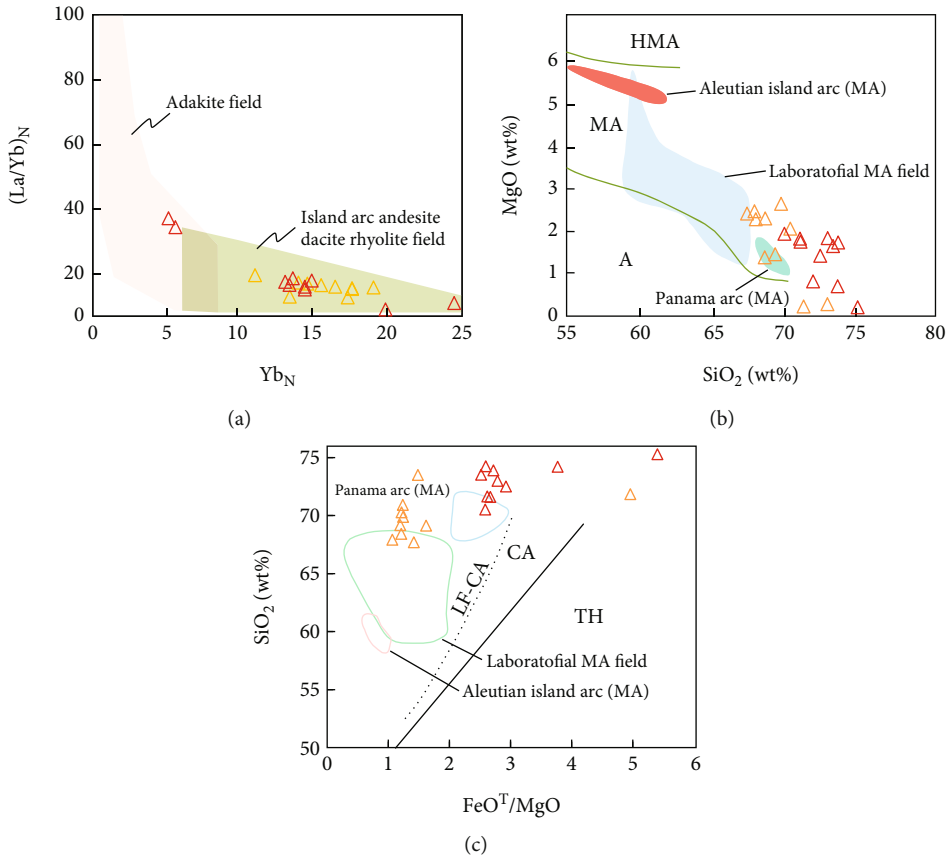

FIGURE 11: (a) $(La/Yb)_N$ vs. Yb_N diagram (after [58]). (b, c) SiO_2 vs. MgO and FeO^T/MgO diagrams (simplified after [64, 68]). HMA: high-Mg-andesitic/dioritic rocks; MA: Mg-andesitic/dioritic rocks; A: lower (or non)-Mg-andesitic/dioritic rocks; CA: calc-alkaline; TH: tholeiitic; LF-CA: low Fe-calc-alkaline. Legend is shown in Figure 6.

6.58 wt%, mean = 3.49), with an average $Fe_2O_3{}^T + TiO_2 +$ MnO + MgO of 4.96, and average Cr and Ni contents of 35.34 and 18.51 ppm, respectively. All samples are plotted in the trondhjemite and granite domains of the normative granitoid classification, suggesting that the TTGs might have developed in the Darongshan pluton.

Previous studies have shown that high- and low-pressure TTGs exhibit different geochemical characteristics such as fractionated REE patterns, Eu anomalies, and Sr/Y ratios (e.g., [28, 54–56]). In general, the geochemical characteristics of high-pressure TTGs are similar to those of typical adakitic rocks [28, 55, 57], while low-pressure TTGs are characterized by low-fractionated REE patterns (or nearly flat REE patterns), a negative Eu anomaly, lower Sr, and higher HREE and Y [26, 55, 56, 58]. High-pressure TTGs include the refractory residual remnants Ga±Hb±Cpx±Opx without residual plagioclase in the source region, while low-pressure TTGs show refractory residual remnants with plagioclase, resulting in a low-fractionated REE pattern and a significantly negative Eu anomaly [54, 56, 59].

The Darongshan granitoids are characterized by a low-fractionated REE pattern, clear negative Eu anomaly ($Eu/Eu^* = 0.27 – 0.67$), high HREE (mean = 19.03) and Y (mean = 27.00), and low Sr (mean = 74.37). The geochemical characteristics of the Darongshan granitoid samples are therefore analogous to those of low-pressure TTGs (Figure 7; [29, 56]). The samples fall mainly in the island-arc andesite–dacite–rhyolite series (ADR) region of the $(La/Yb)_N$ vs. Yb_N diagram (Figure 11(a)), thus showing entirely different characteristics compared to those of typical adakitic rocks.

Several geodynamic mechanisms have been proposed to explain the genesis of TTGs. Common mechanisms include (1) material from the partial melting of subducted oceanic crust reacting with mantle peridotite during its upwards migration to the mantle wedge (e.g., [60–62]) (the most important phenomenon indicating this mechanism is the increased MgO content that occurs in the magma during this process [63–65]) and (2) partial melting of thickened continental crust (e.g., [57, 66, 67]), which is not accompanied by an increase in the MgO content [65, 68]. Experimental petrological studies have supported these genetic mechanisms (e.g., [69–71]). Therefore, the MgO content is a key parameter for identifying subduction slabs and continental crust melts in TTGs (e.g., [26, 72–75]). Recently, Deng et al. [64, 68] suggested the minimum possible MgO% for a given SiO_2% value, based on an experiment investigating magnesian andesitic/dioritic magmas (Table S5; [64, 68]). The Darongshan granitoid samples are plotted in or near the MA area on the SiO_2 vs. MgO diagram (Figure 11(b))

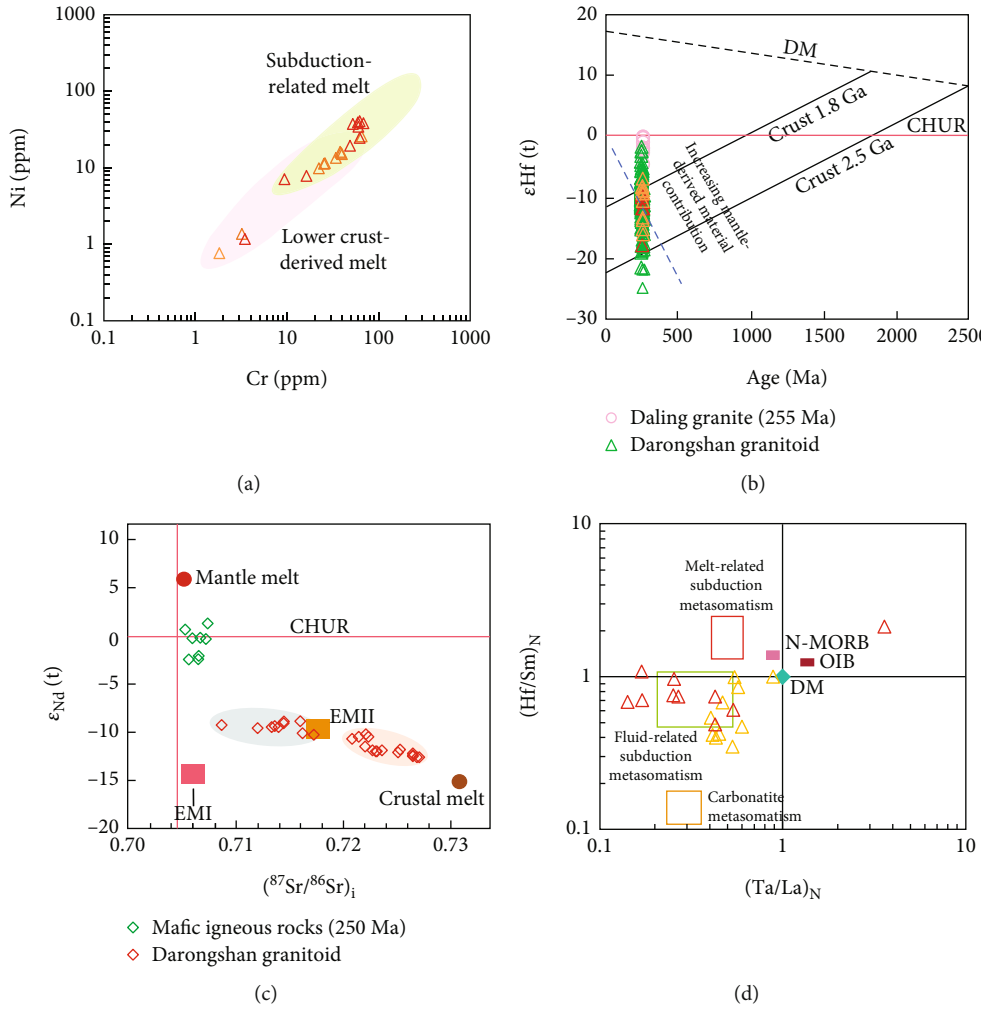

FIGURE 12: (a) Cr vs. Ni diagram (after [121]). (b) Zircon U–Pb age versus $\varepsilon_{Hf}(t)$ diagram. Hf isotopic data for the Daling granite are from Wen and Pang [72]. DM: depleted mantle. Data sources are referenced in Table S6 of the Supplementary Materials. (c) Initial $\varepsilon_{Hf}(t)$ vs. $(^{87}Sr/^{86}Sr)_i$ diagram. The Sr–Nd isotopic data describing the Darongshan granitoid and mafic igneous rocks (250 Ma) are from Qi et al. [30], Fang [122], Wang et al. [43], Li et al. [24], and Qin et al. [78, 100]. Data sources are referenced in Table S7 of the Supplementary Materials. (d) $(Ta/La)_N$ vs. $(Hf/Sm)_N$ diagram (after [79]). Legend is shown in Figure 6.

and in the calc-alkaline or low-Fe calc-alkaline fields in the SiO_2 vs. FeO^T/MgO discrimination diagram (Figure 11(c)). Thus, the granitoid displays MA-like features, implying that it may have undergone subduction-slab melting. In addition, other characteristics of slab melts, such as the relatively high Mg#, Ni, and Cr contents that are attributed to the melting conditions, and the extent of the interaction with the mantle peridotite [76], are observed in almost all samples examined in this study, with the Mg#>50 (Table S1) and relatively high corresponding Ni (mean = 21.48) and Cr (mean = 40.36) suggesting that the slab melts may have been subjected to mantle peridotite assimilation (Figure 12(a)).

The $\varepsilon_{Hf}(t)$ values that were obtained for the Darongshan granitoid range from -24.9 to -1.8 (Table S6). The Hf isotopic data from the granitoid are plotted between the CHUR line and the lower crust evolution region on the $\varepsilon_{Hf}(t)$ vs. U–Pb age diagram (Figure 12(b)), and combined with the zircon $\varepsilon_{Hf}(t)$ values (-4.7 to -0.2) for the Daling granite in northern Hainan Island [77] and the $\varepsilon_{Nd}(t)$ values (-2.61 to +1.10) for mafic igneous rocks in southern Guangxi [78], these results suggest contribution from a relatively depleted ($\varepsilon_{Hf}(t) > 0$) mantle source such as juvenile crust, lithospheric mantle, or asthenosphere mantle. However, no evidence of juvenile crust growth has been observed for the Permian–Triassic period in the study area, indicating the involvement of juvenile mantle-derived materials. Darongshan granitoid shows higher $(^{87}Sr/^{86}Sr)_i$ values and lower $\varepsilon_{Nd}(t)$ values, which range from 0.7086 to 0.7272 and -12.70 to -9.00, respectively (Table S7). The $(^{87}Sr/^{86}Sr)_i$ vs. $\varepsilon_{Nd}(t)$ diagram (Figure 12(c)) indicates that the samples are likely originated in enriched mantle (EMII), and the low $(Hf/Sm)_N$ (0.35 to 2.11) and $(Ta/La)_N$ (0.14 to 3.58) ratios of these rocks suggest that the mantle source has been metasomatized by fluid/melt released from the subducted slab (Figure 12(d), [79]). Peraluminous minerals (such as tourmaline and garnet) and characteristics (A/CNKD>1.1) may be related to the

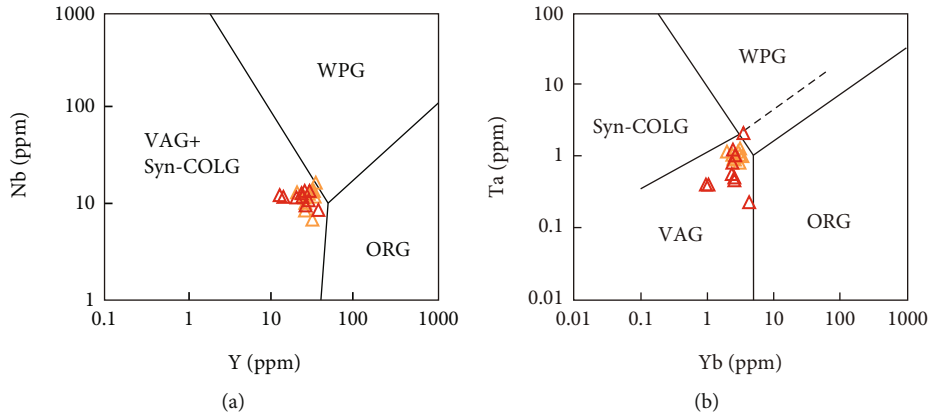

Figure 13: (a) Y vs. Nb and (b) Yb vs. Ta discrimination diagram for the Darongshan granitoid [123]. VAG = volcanic arc granite; Syn-COLG = syn-collision granite; Post-COLG = postcollision granite; WPG = within plate granite; ORG = oceanic ridge granite. Legend is shown in Figure 6.

melting of pelitic or semipelitic rocks in the subduction zone (e.g., [80–83]). The calcic to alkali-calcic trend observed in the Darongshan granitoids (Figure 6(f)) suggests that they may have resulted from mixed magmas, indicating that the Darongshan pluton developed mafic microgranular enclaves.

In summary, the magma generation of the Darongshan granitoid correlates with fluid/melt released from the subducted slab that is then assimilated and mixed with mantle peridotite during ascent.

6.3. Tectonic Implications. During the early Mesozoic, the SCB experienced intense tectonic-magmatic activity, forming a large granite belt (e.g., [15, 16, 30, 84]). The Darongshan granitoids were formed at 262–230 Ma (Figure 10; Table S4), with the most intense magmation occurring at ca. 250 Ma. The rocks are enriched in LILE (e.g., Rb, Th, U, K, and Pb) and demonstrate relative HFSE deficits (e.g., Nb, Ta, P, and Ti) in terms of trace elements, indicating arc-related affinities with subduction zones (Figure 13; [24, 40, 84]). Combined with studies of nearby Indosinian igneous rocks, such as the Wuzhishan granites in Hainan [10], the arc volcanic granites of southern Hunan [85], the Pingxiang volcanic rocks in southwest Guangxi, the arc volcanic deposits in the Youjiang Basin [32, 86], and the arc granites and volcanic rocks of southern Guangxi [24, 45], we tentatively conclude that the Darongshan granitoid may have formed in a continental arc environment (e.g., [37, 43, 87, 88]). Similar scenarios have also been reported for the Piaochi granitoid in the Qinling orogen [89] and the Changshan–Ailaoshan granitoids in Yunnan Province [90].

Regional geodynamic studies have shown that the top-to-the-north nappes in northeast Vietnam and top-to-the-north shearing in the Yunkai massif that occurred during the Permian–Middle Triassic are possibly linked to the subduction and collision of the Indochina Block (ICB) beneath the SCB [91–93]. The NE–SW extrusive deformation that occurred in the Dulong–Song tectonic dome along the Sino–Vietnamese border during the Middle Triassic was related to the closure of the Paleo-Tethys Ocean, which resulted in the northward subduction of the ICB [4, 86, 94]. The magmatic record shows that arc volcanic-intrusive rock assemblages developed in the Pingxiang area in southwest Guangxi and the northern part of Vietnam during the Permian–Early Triassic, and these rocks have been shown to have formed continental marginal arcs in association with oceanic subduction [95, 96]. Notably, Early–Middle Triassic island-arc andesites that are associated with subduction ablation on the southwestern margin of the Youjiang Basin [97] can be connected to the Late Permian island-arc volcanic rocks in Pingxiang [98, 99] and the Late Permian–Middle Triassic island-arc volcanic rocks of Qinzhou–Fangchenggang, which form a magmatic arc belt [100]. This belt may represent the subduction of the eastern Paleo-Tethys Ocean [97]. The sedimentary record shows that the Devonian strata in the Qinzhou–Fangchenggang trough and the Paleo-Tethys oceanic basin in western Yunnan Province were both deposited in the same deepwater environment [101, 102]. Moreover, the Permian Qinzhou–Fangchenggang area shows marine sedimentation that is similar to that of Jinshajiang–Ailaoshan(e.g., [16, 103]). Permian radiolaria silicalite and siliceous mudstone are observed, and the radiolarian composition is characteristic of ocean or deep-sea fauna (i.e., the presence of abundant Pseudotormentus and Albaillellaria), implying that the Qinzhou–Fanchenggang Basin was most likely part of the Paleo-Tethys Ocean branch ocean basin [104]. Contrarily, zircon U–Pb age analyses of the sedimentary rocks in the Qinzhou–Fanchenggang area and Youjiang Basin suggest a Permian–Triassic orogenic event that followed the subduction of the Paleo-Tethys branch ocean, as well as the subsequent collision of the ICB with the SCB [18, 105]. Based on the aforementioned analysis, we propose that the subduction of the eastern Paleo-Tethys Ocean occurred in southern Guangxi during the Early Indosinian.

Recently, zircon U–Pb chronology and Sm–Nd isotope studies have suggested that the Bangxi ophiolite on central

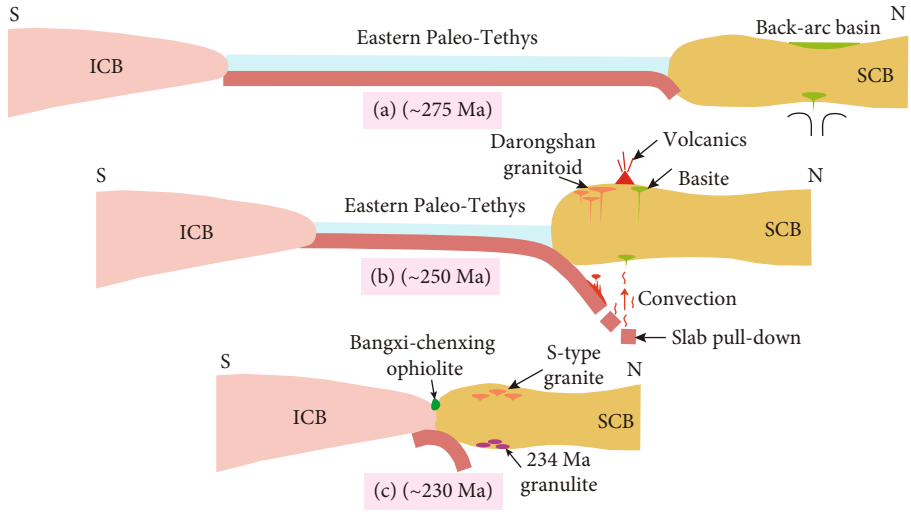

Figure 14: Tectonic evolution model for the eastern Paleo-Tethys during the Early Permian to Late Triassic: (a) earliest Permian: back-arc basin setting [24], north-direction subduction of the eastern Paleo-Tethys [91–93]; (b) earliest Triassic: subducted oceanic crust was further enhanced ca. 250 Ma, with a series of phenomena such as slab melting, breakup, and foundering (in response to a significantly increased geotherm, a major magmatic event occurred in South China [24, 93]); (c) Middle to Late Triassic: amalgamation and initial collision of the SCB and ICB [24, 95, 112].

Hainan Island may be the easternmost oceanic crust remnant of the Paleo-Tethys Ocean [14, 106]. The Bangxi–Chenxing suture zone is also considered to be the eastern extension of the Song Chay suture zone in northeast Vietnam [20, 107, 108]. The ophiolites of the Jinshajiang–Ailaoshan–Song Ma suture zone have the same Sm–Nd and U–Pb age (ca. 340–360 Ma) as the Bangxi–Chenxing ophiolite (e.g., [7, 109, 110]). Thus, the Bangxi–Chenxing suture zone may be the easternmost section of the Jinshajiang–Ailaoshan–Song Ma branch of the Paleo-Tethys Ocean (e.g., [16, 24, 38]). The inherited zircon ages of the Shiwandashan granite in Guangxi (363–314 Ma) and Wuzhishan granite in Hainan (366–312 Ma) were both recorded during this episode [10, 17]. Combined with the sedimentary, magmatic, tectonic, and metamorphic records of adjacent areas, the northward subduction of the eastern Paleo-Tethys oceanic crust probably began approximately 275 Ma (Figure 14(a); e.g., [13, 45, 91, 94]). The foundering of the flab-slab likely occurred ca. 250 Ma (Figure 14(b)), resulting in strong upwelling of the asthenospheric mantle and mafic intra- and/or underplating. A major magmatic event occurred in South China in response to the significant increase in geotherms. In addition to the Darongshan pluton, acidic volcanic rocks are present in the Lang Son area of Vietnam (252–250 Ma; [111]), Changzheng granite in Hainan (ca. 251 Ma; [44]), and rocks in the Longzhou–Chongzuo of Guangxi (ca. 250 Ma; [78]). Significantly, the zircon SHRIMP U–Pb age of eclogite in the Song Ma suture zone is 230.5 ± 8.2 Ma [112]. Clear changes in the sediment sources of clastic rocks on the eastern and western sides of the Ailaoshan suture zone [113] during the Middle–Late Triassic (ca. 237 Ma) suggest that the subduction of the eastern Paleo-Tethys Ocean may have ended ca. 230 Ma, eventually forming the Jinshajiang–Ailaoshan–Song Ma–Bangxi–Chenxing suture zone (Figure 14(c)).

7. Conclusion

Based on the mineralogy, geochemistry, zircon U–Pb ages, and zircon Hf isotopic analysis of the Darongshan granitoid, the following conclusions are proposed:

(1) The LA-ICP-MS U–Pb zircon analysis results indicate that the Darongshan pluton was formed at 249.9 ± 2.6 Ma

(2) The magma from which the Darongshan granitoid was formed was originally fluid/melt, which was released from the subducted slab and assimilated and mixed with mantle peridotite during ascent

(3) The formation of the Darongshan pluton is related to the oceanic subduction of the eastern Paleo-Tethys, with subduction likely ending during the Middle to Late Triassic

Abbreviations

ICB: Indochina Block
SCB: South China Block
MA: Mg-andesitic/dioritic rocks
TTGs: Tonalite–trondhjemite–granodiorites.

Data Availability

The datasets used or analyzed during the current study are available from the corresponding author on reasonable request.

Conflicts of Interest

The authors declare no conflict of interest regarding the publication of this article.

Authors' Contributions

MT was a major contributor in writing the manuscript. YD processed the data. MT and CZ produced the charts for this article. SD checked the article for errors and made corrections. All authors read and approved the final manuscript.

Acknowledgments

This study was supported by the China Geophysical Fields and Metallogenic Relationships (KD-[2020]-XZ-044) project. We thank Ms. Baoling Huang from the Key Laboratory of Orogenic Belts and Crustal Evolution, Ministry of Education, Peking University, for the assistance in the rock analysis.

Supplementary Materials

Table S1: major elements (%) and trace and rare earth elements (ppm) of the Darongshan granitoid. Table S2: zircon U–Th–Pb isotopic analysis of the Darongshan granitoid in southeastern Guangxi. Table S3: zircon Hf isotopic analysis of the Darongshan granitoid in southeastern Guangxi. Table S4: brief summary of the zircon U–Pb chronology data from Darongshan pluton. Table S5: experimentally suggested lowest MgO content at given SiO_2 contents for MA magma. Table S6: brief summary of zircon Hf isotopic compositions in the Darongshan granitoid. Table S7: brief summary of the whole-rock Sr–Nd isotopic compositions in the Darongshan pluton. *(Supplementary Materials)*

References

[1] S. K. Acharyya, "Break-up of the greater Indo-Australian continent and accretion of blocks framing South and East Asia," *Journal of Geodynamics*, vol. 26, no. 1, pp. 149–170, 1998.

[2] I. Metcalfe, "Gondwana dispersion and Asian accretion: tectonic and palaeogeographic evolution of eastern Tethys," *Journal of Asian Earth Sciences*, vol. 66, pp. 1–33, 2013.

[3] I. Metcalfe, R. Hall, and J. D. Holloway, "Palaeozoic and Mesozoic geological evolution of the SE Asian region: multidisciplinary constraints and implications for biogeography," in *Biogeography and Geological Evolution of SE Asia*, pp. 25–41, Backhuys Publishers, Amsterdam, The Netherlands, 1998.

[4] I. Metcalfe, "Palaeozoic and Mesozoic tectonic evolution and palaeogeography of East Asian crustal fragments: the Korean peninsula in context," *Gondwana Research*, vol. 9, no. 1-2, pp. 24–46, 2006.

[5] I. Metcalfe, C. M. Henderson, and K. Wakita, "Lower Permian conodonts from Palaeo-Tethys Ocean plate stratigraphy in the Chiang Mai-Chiang Rai suture zone, Northern Thailand," *Gondwana Research*, vol. 44, pp. 54–66, 2017.

[6] K. Wakita and I. Metcalfe, "Ocean plate stratigraphy in East and Southeast Asia," *Journal of Asian Earth Sciences*, vol. 24, no. 6, pp. 679–702, 2005.

[7] P. Jian, D. Liu, A. Kröner et al., "Devonian to Permian plate tectonic cycle of the Paleo-Tethys Orogen in Southwest China (II): insights from zircon ages of ophiolites, arc/back-arc assemblages and within-plate igneous rocks and generation of the Emeishan CFB province," *Lithos*, vol. 113, no. 3-4, pp. 767–784, 2009.

[8] M. Faure, C. Lepvrier, V. VanNguyen, T. VanVu, W. Lin, and Z. Chen, "The South China Block-Indochina collision: where, when, and how?," *Journal of Asian Earth Sciences*, vol. 79, pp. 260–274, 2014.

[9] H. Liu, Y. Wang, Z. Li, J. W. Zi, and P. Huangfu, "Geodynamics of the Indosinian orogeny between the South China and Indochina blocks: insights from latest Permian-Triassic granitoids and numerical modeling," *Geological Society of America Bulletin*, vol. 130, no. 7-8, pp. 1289–1306, 2018.

[10] X. Y. Chen, Y. J. Wang, W. M. Fan, F. F. Zhang, T. P. Peng, and Y. Z. Zhang, "Zircon LA-ICP-MS U-Pb dating of granitic gneisses from Wuzhishan area, Hainan, and geological significances," *Geochimica*, vol. 40, no. 5, pp. 454–463, 2011.

[11] S. N. Wen, X. Q. Liang, W. M. Fan et al., "Zircon U-Pb ages, Hf isotopic composition of Zhizhong granitic intrusion in Ledong area of Hainan Island and their tectonic implications," *Geotectonica et Metallogenia*, vol. 37, no. 2, pp. 294–307, 2013.

[12] C. Xie, J. Zhu, S. Ding, Y. Zhang, T. A. Fu, and Z. Li, "Identification of Hercynian shoshonitic intrusive rocks in central Hainan Island and its geotectonic implications," *Chinese Science Bulletin*, vol. 51, no. 20, pp. 2507–2519, 2006.

[13] Q. Li, W. Lin, Y. Wang et al., "Detrital zircon U-Pb age distributions and Hf isotopic constraints of the Ailaoshan-Song Ma suture zone and their paleogeographic implications for the Paleo-Tethys evolution," *Earth-Science Reviews*, vol. 221, article 103789, 2021.

[14] X. H. Li, H. Zhou, S. L. Chung et al., "Geochemical and Sm-Nd isotopic characteristics of metabasites from central Hainan Island, South China and their tectonic significance," *Island Arc*, vol. 11, pp. 193–205, 2002.

[15] X. Zhang, H. Li, C. K. Lai, and Q. Tan, "New sedimentary constraints for the Late Devonian north-dipping Paleo-Tethys subduction and its eastern continuation on Hainan Island, South China," *Marine and Petroleum Geology*, vol. 142, article 105743, 2022.

[16] Y. Zhou, Y. Yan, H. Liu et al., "U-Pb isotope geochronology of syntectonic granites from Hainan Island, South China: constraints on tectonic evolution of the eastern Paleo-Tethys Ocean," *Journal of Ocean University of China*, vol. 19, no. 6, pp. 1315–1330, 2020.

[17] C. H. Chen, P. S. Hsieh, C. Y. Lee, and H. W. Zhou, "Two episodes of the Indosinian thermal event on the South China Block: constraints from LA-ICPMS U-Pb zircon and electron microprobe monazite ages of the Darongshan S-type granitic suite," *Gondwana Research*, vol. 19, no. 4, pp. 1008–1023, 2011.

[18] L. S. Hu, Y. S. Du, P. A. Cawood et al., "Drivers for late Paleozoic to early Mesozoic orogenesis in South China: constraints from the sedimentary record," *Tectonophysics*, vol. 618, pp. 107–120, 2014.

[19] D. R. Xu, B. Xia, P. C. Li, G. H. Chen, C. Ma, and Y. Q. Zhang, "Protolith natures and U-Pb sensitive high mass-resolution ion microprobe (SHRIMP) zircon ages of the metabasites in Hainan Island, South China: implications for geodynamic evolution since the late Precambrian," *Island Arc*, vol. 16, no. 4, pp. 575–597, 2007.

[20] M. Faure, W. Lin, Y. Chu, and C. Lepvrier, "Triassic tectonics of the southern margin of the South China Block," *Comptes Rendus Geoscience*, vol. 348, no. 1, pp. 5–14, 2016.

[21] C. Lepvrier, N. Van Vuong, H. Maluski, P. T. Thi, and T. Van Vu, "Indosinian tectonics in Vietnam," *Comptes Rendus Geoscience*, vol. 340, no. 2-3, pp. 94–111, 2008.

[22] T. F. Wan, *The Tectonics of China*, Geological Publishing House, Beijing, China, 2011.

[23] J. X. Cai and K. J. Zhang, "A new model for the Indochina and South China collision during the Late Permian to the Middle Triassic," *Tectonophysics*, vol. 467, no. 1–4, pp. 35–43, 2009.

[24] Y. J. Li, J. H. Wei, M. Santosh, J. Tan, L. B. Fu, and S. Q. Zhao, "Geochronology and petrogenesis of Middle Permian S-type granitoid in southeastern Guangxi Province, South China: implications for closure of the eastern Paleo-Tethys," *Tectonophysics*, vol. 682, pp. 1–16, 2016.

[25] J. D. Clemens, L. M. Yearron, and G. Stevens, "Barberton (South Africa) TTG magmas: geochemical and experimental constraints on source-rock petrology, pressure of formation and tectonic setting," *Precambrian Research*, vol. 151, no. 1-2, pp. 53–78, 2006.

[26] J. F. Deng, Y. F. Feng, Y. J. Di, S. G. Su, Q. H. Xiao, and G. Y. Wu, *Geotectonics of Intrusion Rocks in China*, Geological Publishing House, Beijing, 2017.

[27] H. Martin, R. H. Smithies, R. Rapp, J. F. Moyen, and D. Champion, "An overview of adakite, tonalite-trondhjemite-granodiorite (TTG), and sanukitoid: relationships and some implications for crustal evolution," *Lithos*, vol. 79, no. 1-2, pp. 1–24, 2005.

[28] J. F. Moyen and H. Martin, "Forty years of TTG research," *Lithos*, vol. 148, pp. 312–336, 2012.

[29] R. P. Rapp and E. B. Watson, "Dehydration melting of metabasalt at 8–32 kbar: implications for continental growth and crust-mantle recycling," *Journal of Petrology*, vol. 36, no. 4, pp. 891–931, 1995.

[30] C. S. Qi, X. G. Deng, W. X. Li, X. H. Li, Y. H. Yang, and L. W. Xie, "Origin of the Darongshan-Shiwandashan S-type granitoid belt from southeastern Guangxi: geochemical and Sr-Nd-Hf isotopic constraints," *Acta Petrologica Sinica*, vol. 23, no. 2, pp. 403–412, 2007.

[31] X. Y. Jiang and X. H. Li, "In situ zircon U-Pb and Hf-O isotopic results for ca. 73 Ma granite in Hainan Island: implications for the termination of an Andean-type active continental margin in southeast China," *Journal of Asian Earth Sciences*, vol. 82, pp. 32–46, 2014.

[32] J. Li, G. Zhao, S. T. Johnston et al., "Permo-Triassic structural evolution of the Shiwandashan and Youjiang structural belts, South China," *Journal of Structural Geology*, vol. 100, pp. 24–44, 2017.

[33] Z. X. Li and X. H. Li, "Formation of the 1300-km-wide intracontinental orogen and postorogenic magmatic province in Mesozoic South China: a flat-slab subduction model," *Geology*, vol. 35, no. 2, pp. 179–182, 2007.

[34] Y. F. Zheng, W. J. Xiao, and G. Zhao, "Introduction to tectonics of China," *Gondwana Research*, vol. 23, no. 4, pp. 1189–1206, 2013.

[35] P. Gao, Y. F. Zheng, and Z. F. Zhao, "Triassic granites in South China: a geochemical perspective on their characteristics, petrogenesis, and tectonic significance," *Earth-Science Reviews*, vol. 173, pp. 266–294, 2017.

[36] Y. Wang, A. Zhang, P. A. Cawood et al., "Geochronological, geochemical and Nd-Hf-Os isotopic fingerprinting of an early Neoproterozoic arc-back-arc system in South China and its accretionary assembly along the margin of Rodinia," *Precambrian Research*, vol. 231, pp. 343–371, 2013.

[37] X. Zhou, T. Sun, W. Shen, L. Shu, and Y. Niu, "Petrogenesis of Mesozoic granitoids and volcanic rocks in South China: a response to tectonic evolution," *Episodes Journal of International Geoscience*, vol. 29, no. 1, pp. 26–33, 2006.

[38] S. J. Jiao, X. H. Li, H. Q. Huang, and X. G. Deng, "Metasedimentary melting in the formation of charnockite: petrological and zir-con U-Pb-Hf-O isotope evidence from the Darongshan S-type granitic complex in southern China," *Lithos*, vol. 239, pp. 217–233, 2015.

[39] C. Y. Zeng, Y. Z. Zhou, Y. Zheng et al., "Plate tectonism of Qinzhou Bay-Hangzhou Bay juncture orogenic belt (South China) before Mesozoic tectonic transition event," *Earth Science Frontiers*, vol. 22, no. 2, pp. 54–63, 2015.

[40] W. B. Wang, J. H. Li, Y. J. Xin, H. S. Sun, and Y. Q. Yu, "Zircon LA-ICP-MS U-Pb dating and geochemical analysis of the Darongshan-Shiwandashan granitoids in southwestern South China and their geological implications," *Acta Geoscientica Sinica*, vol. 39, no. 2, pp. 179–188, 2018.

[41] L. Zhao, F. Guo, W. Fan, C. Li, X. Qin, and H. Li, "Crustal evolution of the Shiwandashan area in South China: zircon U-Pb-Hf isotopic records from granulite enclaves in Indo-Sinian granites," *Chinese Science Bulletin*, vol. 55, no. 19, pp. 2028–2038, 2010.

[42] X. G. Deng, Z. G. Chen, X. H. Li, and D. Y. Liu, "SHRIMP U-Pb zircon dating of the Darongshan-Shiwandashan granitoid belt in southeastern Guangxi, China," *Geological Review*, vol. 50, no. 4, pp. 426–432, 2004.

[43] M. Wang, X. Zhang, D. Pi, and X. Guo, "Zircon U–Pb dating of Pubei granite and strontium isotope from sphalerite of the Xinhua Pb–Zn–(Ag) deposit, Yunkai area of Guangxi Province, South China," *Acta Geochimica*, vol. 35, no. 2, pp. 156–171, 2016.

[44] G. F. Zhao, H. C. Liu, X. Qian et al., "Petrogenesis of Late Permian I-type granites in SE Hainan Island and its tectonic implication for Paleotethyan evolution [in Chinese with English abstract]," *Earth Science*, vol. 43, no. 4, pp. 1321–1332, 2017.

[45] X. F. Qin, Z. Q. Wang, J. Cao, Z. H. Feng, G. A. Hu, and L. Z. Pan, "Petrogenesis of early Indosinian granites from the south-western segment of Qinfang tectonic belt, southern Guangxi: constraints from zircon U-Pb chronology and geochemistry," *Journal of Jilin University*, vol. 43, no. 5, pp. 1471–1488, 2013.

[46] P. Gao, Y. F. Zheng, Y. X. Chen, Z. F. Zhao, and X. P. Xia, "Relict zircon U-Pb age and O isotope evidence for reworking of Neoproterozoic crustal rocks in the origin of Triassic S-type granites in South China," *Lithos*, vol. 300-301, pp. 261–277, 2018.

[47] C. Paton, J. D. Woodhead, J. C. Hellstrom, J. M. Hergt, A. Greig, and R. Maas, "Improved laser ablation U-Pb zircon geochronology through robust downhole fractionation correction," *Geochemistry, Geophysics, Geosystems*, vol. 11, no. 3, article Q0AA06, 2010.

[48] J. Sláma, J. Kosler, D. J. Condon et al., "Plešovice zircon–a new natural reference material for U-Pb and Hf isotopic microanalysis," *Chemical Geology*, vol. 249, no. 1-2, pp. 1–35, 2008.

[49] J. Thompson, S. Meffre, and L. Danyushevsky, "Impact of air, laser pulse width and fluence on U–Pb dating of zircons by

LA-ICPMS," *Journal of Analytical Atomic Spectrometry*, vol. 33, no. 2, pp. 221–230, 2018.

[50] F. Y. Wu, Y. H. Yang, L. W. Xie, J. H. Yang, and P. Xu, "Hf isotopic compositions of the standard zircons and baddeleyites used in U-Pb geochronology," *Chemical Geology*, vol. 234, no. 1-2, pp. 105–126, 2006.

[51] T. G. Griffin, "A formulae-as-types notion of control," *Computer Science*, vol. 3, pp. 47–58, 2000.

[52] J. Blicherttoft, C. Chauvel, and F. Albarède, "Separation of Hf and Lu for high-precision isotope analysis of rock samples by magnetic sector-multiple collector ICP-MS," *Contributions to Mineralogy and Petrology*, vol. 127, no. 3, pp. 248–260, 1997.

[53] M. Y. Tian, Y. J. Di, S. S. Li, and S. Zhang, "Geochemical characteristics and genesis of biotite monzogranite in southeastern Guangxi Province, South China," *Earth*, vol. 10, no. 6, pp. 325–331, 2021.

[54] F. Barker, *Trondhjemites, Dacites and Related Rocks*, Elsevier Scientific Publishing Company, New York, 1979.

[55] N. Petford and M. Atherton, "Na-rich partial melts from newly underplated basaltic crust: the Cordillera Blanca Batholith, Peru," *Journal of petrology*, vol. 37, no. 6, pp. 1491–1521, 1996.

[56] J. F. Deng, C. Liu, Y. J. Di et al., "Discussion on the tonalite-trondhjemite-granodiorite (TTG) petrotectonic assemblage and its subtypes," *Earth Science Frontiers*, vol. 25, no. 6, pp. 42–50, 2018.

[57] M. P. Atherton and N. Petford, "Generation of sodium-rich magmas from newly underplated basaltic crust," *Nature*, vol. 362, no. 6416, pp. 144–146, 1993.

[58] M. S. Drummond and M. J. Defant, "Derivation of some modern arc magmas by melting of young subducted lithosphere," *Nature*, vol. 347, no. 6294, pp. 662–665, 1990.

[59] W. Johannes and F. Holtz, *Petrogensis and Experimental Petrology of Granitic Rocks*, Minerals and Rocks, Springer-Verlag, Berlin, 1996.

[60] M. S. Drummond, M. J. Defant, and P. K. Kepezhinskas, "Petrogenesis of slab-derived trondhjemite–tonalite–dacite/adakite magmas," *Earth and Environmental Science Transactions of the Royal Society of Edinburgh*, vol. 87, no. 1-2, pp. 205–215, 1996.

[61] J. F. Moyen, "The composite Archaean grey gneisses: petrological significance, and evidence for a non-unique tectonic setting for Archaean crustal growth," *Lithos*, vol. 123, no. 1-4, pp. 21–36, 2011.

[62] F. G. Sajona, R. C. Maury, M. Pubellier, J. Leterrier, H. Bellon, and J. Cotten, "Magmatic source enrichment by slab-derived melts in a young post-collision setting, Central Mindanao (Philippines)," *Lithos*, vol. 54, no. 3-4, pp. 173–206, 2000.

[63] M. J. Defant, P. M. Richerson, J. Z. Deboer et al., "Dacite genesis via both slab melting and differentiation: petrogenesis of La Yeguada volcanic complex, Panama," *Journal of Petrology*, vol. 32, no. 6, pp. 1101–1142, 1991.

[64] J. F. Deng, C. Liu, Y. F. Feng et al., "High magnesian andesitic/dioritic rocks (HMA) and magnesian andesitic/dioritic rocks (MA): two igneous rock types related to oceanic subduction," *Geology in China*, vol. 37, no. 4, pp. 1112–1118, 2010.

[65] J. F. Deng, Q. H. Xiao, S. G. Su et al., "Igneous petrotectonic assemblages and tectonic settings: a discussion," *Geological Journal of China Universities*, vol. 13, no. 3, pp. 392–402, 2007.

[66] K. C. Condie, "TTGs and adakites: are they both slab melts?," *Lithos*, vol. 80, no. 1-4, pp. 33–44, 2005.

[67] Y. He, S. Li, J. Hoefs, F. Huang, S. A. Liu, and Z. Hou, "Post-collisional granitoids from the Dabie orogen: new evidence for partial melting of a thickened continental crust," *Geochimica et Cosmochimica Acta*, vol. 75, no. 13, pp. 3815–3838, 2011.

[68] J. Deng, M. F. Flower, C. Liu, X. Mo, S. Su, and Z. Wu, "Nomenclature, diagnosis and origin of high-magnesian andesits (HMA) and magnesian andesits (MA): a review from petrographic and experimental data," *Geochimica et Cosmochimica Acta*, vol. 73, no. 13-1, article A279, 2009.

[69] G. Prouteau, B. Scaillet, M. Pichavant, and R. Maury, "Evidence for mantle metasomatism by hydrous silicic melts derived from subducted oceanic crust," *Nature*, vol. 410, no. 6825, pp. 197–200, 2001.

[70] R. H. Smithies and D. C. Champion, "The Archaean high-Mg diorite suite: links to tonalite–trondhjemite–granodiorite magmatism and implications for early Archaean crustal growth," *Journal of Petrology*, vol. 41, no. 12, pp. 1653–1671, 2000.

[71] X. L. Xiong, J. Adam, and T. H. Green, "Rutile stability and rutile/melt HFSE partitioning during partial melting of hydrous basalt: implications for TTG genesis," *Chemical Geology*, vol. 218, no. 3-4, pp. 339–359, 2005.

[72] Y. F. Feng, X. F. Yao, Y. Q. Wei et al., "Yanshanian (J-K) TTG rocks assemblage and its geological significance, Changle-Nan'ao tectonic belt," *Acta Petrologica Sinica*, vol. 30, no. 11, pp. 3315–3333, 2014.

[73] Y. D. Liu, X. L. Su, H. Y. Cheng, J. F. Zhang, X. Li, and F. L. Liu, "Geochronological and geochemical characteristics of the Caledonian Longquan pluton in southern Zhejiang, and their geological significance," *Journal of Geomechanics*, vol. 28, no. 2, pp. 237–256, 2022.

[74] R. H. Smithies, "The Archaean tonalite-trondhjemite-granodiorite (TTG) series is not an analogue of cenozoic adakite," *Earth and Planetary Science Letters*, vol. 182, no. 1, pp. 115–125, 2000.

[75] G. M. Yogodzinski, R. W. Kay, O. N. Volynets, A. V. Koloskov, and S. M. Kay, "Magnesian andesite in the western Aleutian Komandorsky region: implications for slab melting and processes in the mantle wedge," *Geological Society of America Bulletin*, vol. 107, no. 5, pp. 505–519, 1995.

[76] H. Martin, "Adakitic magmas: modern analogues of Archaean granitoids," *Lithos*, vol. 46, no. 3, pp. 411–429, 1999.

[77] S. Wen and C. Pang, "Petrogenesis of the Late Permian Daling intrusion on Hainan Island: constraints from in-situ zircon Hf isotopes," *Journal of Guilin University of Technology*, vol. 38, no. 4, pp. 654–662, 2018.

[78] X. F. Qin, Z. Q. Wang, Y. L. Zhang, L. Z. Pan, G. Hu, and F. S. Zhou, "Geochemistry of Permian mafic igneous rocks from the Napo-Qinzhou tectonic belt in southwest Guangxi, Southwest China: implications for arc-back arc basin magmatic evolution," *Acta Geologica Sinica-English Edition*, vol. 86, no. 5, pp. 1182–1199, 2012.

[79] M. R. LaFlèche, G. Camire, and G. A. Jenner, "Geochemistry of post-Acadian, Carboniferous continental intraplate basalts from the Maritimes basin, Magdalen Islands, Quebec, Canada," *Chemical Geology*, vol. 148, no. 3-4, pp. 115–136, 1998.

[80] C. H. Chen, W. Lin, C. Y. Lan, and C. Y. Lee, "Geochemical, Sr and Nd isotopic characteristics and tectonic implications for three stages of igneous rock in the Late Yanshanian (cretaceous) orogeny, SE China," *Earth and Environmental Science Transactions of The Royal Society of Edinburgh*, vol. 95, no. 1-2, pp. 237–248, 2004.

[81] Y. F. Feng, J. F. Deng, and Q. H. Xiao, *The Granitoids, Geochronology, Rock Assemblages, Tectonic and Evolution of the Changle-Nan'ao Tectonic Belt*, Geological Publishing House, Beijing, 2013.

[82] F. Holtz and P. Barbey, "Genesis of peraluminous granites II. Mineralogy and chemistry of the Tourem complex (North Portugal). Sequential melting vs. restite unmixing," *Journal of Petrology*, vol. 32, no. 5, pp. 959–978, 1991.

[83] C. Y. Lan, B. M. Jahn, S. A. Mertzman, and T. W. Wu, "Subduction-related granitic rocks of Taiwan," *Journal of Southeast Asian Earth Sciences*, vol. 14, no. 1-2, pp. 11–28, 1996.

[84] Y. S. Yuan, *Geochemistry and Tectonic Setting of the Yongan Granitoid Pluton in Southeastern Guangxi, [M.S. thesis]*, China University of Geosciences, Beijing China, 2016.

[85] X. H. Li, Z. X. Li, W. X. Li, and Y. Wang, "Initiation of the Indosinian Orogeny in South China: evidence for a Permian magmatic arc on Hainan Island," *The Journal of geology*, vol. 114, no. 3, pp. 341–353, 2006.

[86] Y. S. Du, H. Huang, J. H. Yang et al., "The basin translation from late Paleozoic to Triassic of the Youjiang basin and its tectonic signification," *Geological Review*, vol. 59, no. 1, pp. 1–11, 2013.

[87] H. Huang, *The Basin Translation from the Late Paleozoic to Middle Triassic of the Youjiang Basin: Evidence from Geochemistry of Sedimentary and Volcanic Rocks, [Ph.D. thesis]*, China University of Geosciences, Wuhan China, 2013.

[88] G. Y. Zhao, X. F. Qin, Z. Q. Wang et al., "Geochronology, geochemistry and geological significance of Gabbros from Xindi-Anping area, Southeastern Guangxi," *Acta Petrologica et Mineralogica*, vol. 35, no. 5, pp. 791–803, 2016.

[89] Z. W. Qin, Y. B. Wu, H. Wang et al., "Geochronology, geochemistry, and isotope compositions of Piaochi S-type granitic intrusion in the Qinling orogen, Central China: Petrogenesis and tectonic significance," *Lithos*, vol. 202-203, pp. 347–362, 2014.

[90] J. Xu, X. P. Xia, Q. Wang et al., "Pure sediment-derived granites in a subduction zone," *Geological Society of America Bulletin*, vol. 134, no. 3-4, pp. 599–615, 2022.

[91] C. Lepvrier, M. Faure, V. N. Van et al., "North-directed Triassic nappes in northeastern Vietnam (east bac Bo)," *Journal of Asian Earth Sciences*, vol. 41, no. 1, pp. 56–68, 2011.

[92] W. Lin, Q. Wang, and K. Chen, "Phanerozoic tectonics of South China block: new insights from the polyphase deformation in the Yunkai massif," *Tectonics*, vol. 27, no. 6, article TC6004, 2008.

[93] Z. Wang, D. Xu, C. Wu, W. Fu, L. Wang, and J. Wu, "Discovery of the late Paleozoic Ocean island basalts (OIB) in Hainan Island and their geodynamic implications," *Acta Petrologica Sinica*, vol. 29, no. 3, pp. 875–886, 2013.

[94] T. Peng, W. Fan, G. Zhao, B. Peng, X. Xia, and Y. Mao, "Petrogenesis of the early Paleozoic strongly peraluminous granites in the Western South China Block and its tectonic implications," *Journal of Asian Earth Sciences*, vol. 98, pp. 399–420, 2015.

[95] Z. L. Li, X. J. Liu, W. J. Xiao et al., "Geochronology, geochemistry and Hf isotopes of volcanic rocks in Pingxiang area, southwest Guangxi: implications for the latest stage of Paleo-Tethyan Ocean northward subuction," *Journal of Geomechanics*, vol. 25, no. 5, pp. 932–946, 2019.

[96] G. Y. Wu, H. R. Wu, D. L. Zhong, G. D. Kuang, and J. Q. Ji, "Volcanic rocks of Paleotethyan oceanic island and island-arc bordering Yunnan and Guangxi, China," *Geoscience*, vol. 14, no. 4, pp. 393–400, 2000.

[97] L. S. Hu, Y. S. Du, J. H. Yang, H. Huang, H. W. Huang, and Z. Q. Huang, "Geochemistry and tectonic significance of Middle Triassic volcanic rocks in Nalong, Guangxi area," *Geological Review*, vol. 58, no. 3, pp. 481–494, 2012.

[98] W. H. He, Y. F. Xiao, X. Ke, Z. X. Zhang, and H. Z. Yao, "The Qinphang basin is a branch basin of the Paleo-Tethys Ocean: evidence from paleontology and sedimentology," in *Joint Meetings on the 12th National Congress of the Palaeontological Society of China (PSC) and the 29th Annual Conference of PSC*, pp. 243-244, Zhengzhou, China, 2018.

[99] G. Y. Wu, J. Q. Ji, S. D. He, and D. L. Zhong, "Early Permian magmatic arc in Pingxiang, Guangxi and its tectonic implications," *Journal of Mineralogy and Petrology*, vol. 22, no. 3, pp. 61–65, 2002.

[100] X. F. Qin, Z. Q. Wang, Y. L. Zhang, L. Z. Pan, G. Hu, and F. S. Zhou, "Geochronology and geochemistry of early Mesozoic acid volcanic rocks from southwest Guangxi: constraints on tectonic evolution of the southwestern segment of Qinzhou-Hangzhou joint belt," *Acta Petrologica Sinica*, vol. 27, no. 3, pp. 794–808, 2011.

[101] J. Yang, P. A. Cawood, Y. Du, H. Huang, and L. Hu, "Detrital record of Indosinian mountain building in SW China: provenance of the Middle Triassic turbidites in the Youjiang basin," *Tectonophysics*, vol. 574-575, pp. 105–117, 2012.

[102] L. Zhao, F. Guo, W. Fan, C. Li, X. Qin, and H. Li, "Origin of the granulite enclaves in Indo-Sinian peraluminous granites, South China and its implication for crustal anatexis," *Lithos*, vol. 150, pp. 209–226, 2012.

[103] S. J. Jiao, J. H. Guo, and S. B. Peng, "Petrogenesis of garnet in the Darongshan-Shiwandashan granitic suite of the South China Block and the metamorphism of the granulite enclave," *Acta Petrologica Sinica*, vol. 29, no. 5, pp. 1740–1758, 2013.

[104] W. P. Ma, "Paleo-Tethys in South China, Permian orogeny and the eastwards extension of interchange domain," *Chinese Journal of Geology*, vol. 31, pp. 105–113, 1996.

[105] X. Y. Chen, Y. J. Wang, Y. Z. Zhang, F. F. Zhang, and S. N. Wen, "Geochemical and geochronological characteristics and its tectonic significance of andesitic volcanic rocks in Chenxing area, Hainan," *Geotectonica et Metallogenia*, vol. 37, no. 2, pp. 99–108, 2013.

[106] J. Liu, M. D. Tran, Y. Tang et al., "Permo-Triassic granitoids in the northern part of the Truong Son belt, NW Vietnam: geochronology, geochemistry and tectonic implications," *Gondwana Research*, vol. 22, no. 2, pp. 628–644, 2012.

[107] Z. Chen, W. Lin, M. Faure, C. Lepvrier, N. Van Vuong, and V. Van Tich, "Geochronology and isotope analysis of the late Paleozoic to Mesozoic granitoids from northeastern Vietnam and implications for the evolution of the South China Block," *Journal of Asian Earth Sciences*, vol. 86, pp. 131–150, 2014.

[108] N. V. Vu□ng, B. T. Hansen, K. Wemmer, C. Lepvrier, V. V. Tích, and T. T. Thắng, "U/Pb and Sm/Nd dating on ophiolitic rocks of the Song Ma suture zone (Northern Vietnam):

evidence for Upper Paleozoic Paleotethyan lithospheric remnants," *Journal of Geodynamics*, vol. 69, pp. 140–147, 2013.

[109] C. K. Lai, S. Meffre, A. J. Crawford et al., "The Central Ailaoshan ophiolite and modern analogs," *Gondwana Research*, vol. 26, no. 1, pp. 75–88, 2014.

[110] R. Y. Zhang, C. H. Lo, X. H. Li, S. L. Chung, T. T. Anh, and T. Van Tri, "U-Pb dating and tectonic implication of ophiolite and metabasite from the Song Ma suture zone, Northern Vietnam," *American Journal of Science*, vol. 314, no. 2, pp. 649–678, 2014.

[111] J. A. Halpin, H. T. Tran, C. K. Lai, S. Meffre, A. J. Crawford, and K. Zaw, "U-Pb zircon geochronology and geochemistry from NE Vietnam: a 'tectonically disputed' territory between the Indochina and South China blocks," *Gondwana Research*, vol. 34, pp. 254–273, 2016.

[112] R. Y. Zhang, C. H. Lo, S. L. Chung et al., "Origin and tectonic implication of ophiolite and eclogite in the Song Ma suture zone between the South China and Indochina blocks," *Journal of Metamorphic Geology*, vol. 31, no. 1, pp. 49–62, 2013.

[113] J. Xu, X. P. Xia, C. Lai, X. Long, and C. Huang, "When did the Paleotethys Ailaoshan Ocean close: new insights from detrital zircon U-Pb age and Hf isotopes," *Tectonics*, vol. 38, no. 5, pp. 1798–1823, 2019.

[114] T. N. Irvine and W. R. A. Baragar, "A guide to the chemical classification of the common volcanic rocks," *Canadian Journal of Earth Sciences*, vol. 8, no. 5, pp. 523–548, 1971.

[115] J. T. O'Connor, "A classification for quartz-rich igneous rocks based on feldspar ratios," *US Geological Survey, Professional Papers*, vol. 525, pp. B79–B84, 1965.

[116] A. Peccerillo and S. R. Taylor, "Geochemistry of Eocene calc-alkaline volcanic rocks from the Kastamonu area, northern Turkey," *Contributions to Mineralogy and Petrology*, vol. 58, no. 1, pp. 63–81, 1976.

[117] P. D. Maniar and P. M. Piccoli, "Tectonic discrimination of granitoids," *Geological Society of America Bulletin*, vol. 101, no. 5, pp. 635–643, 1989.

[118] B. R. Frost, C. G. Barnes, W. J. Collins, R. J. Arculus, D. J. Ellis, and C. D. Frost, "A geochemical classification for granitic rocks," *Journal of Petrology*, vol. 42, no. 11, pp. 2033–2048, 2001.

[119] S. S. Sun and W. F. McDonough, "Chemical and isotopic systematics of oceanic basalts: implications for mantle composition and processes," *Geological Society London Special Publications*, vol. 42, no. 1, pp. 313–345, 1989.

[120] H. Martin and J. F. Moyen, "Secular changes in tonalite-trondhjemite-granodiorite composition as markers of the progressive cooling of earth," *Geology*, vol. 30, no. 4, pp. 319–322, 2002.

[121] Q. Guan, D. C. Zhu, Z. D. Zhao et al., "Crustal thickening prior to 38 Ma in southern Tibet: evidence from lower crust-derived adakitic magmatism in the Gangdese Batholith," *Gondwana Research*, vol. 21, no. 1, pp. 88–99, 2012.

[122] D. Fang, *Geological, Geochemical Characteristics and Petrogenesis of the Wangchong Granitic Super Unit, [M.S. thesis]*, East China University of Technology, Darongshan Area, Guangxi Province, Nanchang China, 2012.

[123] J. A. Pearce, N. B. Harris, and A. G. Tindle, "Trace element discrimination diagrams for the tectonic interpretation of granitic rocks," *Journal of Petrology*, vol. 25, no. 4, pp. 956–983, 1984.